

# Elastic forces on nematic point defects

Eugene C. Gartland, Jr.

*Department of Mathematical Sciences, Kent State University,*

*P.O. Box 5190, Kent, OH 44242-0001 USA*

André M. Sonnet and Epifanio G. Virga

*Dipartimento di Matematica, Istituto Nazionale di Fisica della Materia,*

*Università di Pavia, via Ferrata 1, 27100 Pavia, Italy*

(Dated: August 27, 2001)

We present a general method to compute the elastic forces exerted on nematic point defects: these are the forces that set defects in motion, and so they are especially relevant to defect dynamics, a subject which is recently attracting much interest. These forces are mediated by the distortion introduced by defects in the director field; for example, they are responsible for the attraction between defects of opposite topological charge.

PACS numbers: 61.30.Jf

## I. INTRODUCTION

Understanding defect dynamics is a major challenge in soft matter modelling. The interest in this topic becomes even broader as one considers how well defects in liquid crystals can be paradigms for other singularities in diverse branches of physics, such as cosmology and particle physics (cf. [1] for a lucid and documented account on these similarities). Among all complex ordered media, uniaxial liquid crystals are by far the simplest, as their order parameter is a single unit vector  $\mathbf{n}$ , often called the *director*. Even within liquid crystals, fascinating phenomena such as pairwise annihilation of nematic point defects still lack a comprehensive description. In particular, asymmetries recently observed in the motion of defects with opposite signs of the topological charge are rather puzzling. Cladis and Brand [2] have reported different velocities for a  $+1$  and a  $-1$  defect as they approach each other, the  $+1$  defect moving several times quicker than the  $-1$  defect, so that their annihilation point is not in the middle between their starting positions. No theory is yet available to explain

this experiment.

Though the dynamical theory for liquid crystals goes back to the seminal works of Ericksen [3] and Leslie [4], it has not yet proven fully successful in describing the motion of defects, even—we believe—in its numerical applications. Here we address a crucial question in the development of a sound theory of defect dynamics: how to compute the force exerted on a point defect by the surrounding director field, especially away from equilibrium. We call this force *elastic* because it is in a way mediated by the distortion in the director field. Elastic is, for instance, the interaction force that two or more defects exchange through the intervening director arrangement. These forces can indeed be quite different from their *quasi-static* counterparts, which are evaluated by differentiating with respect to the positions of the defects the minimum elastic free energy computed with all defects held fixed in a given configuration.

In Sec. II, we arrive from first principles at a formula for the elastic force acting on a point defect, which involves Ericksen's stress tensor for liquid crystals. In Sec. III, we apply this formula to compute the interaction force between two defects of opposite topological charge confined within a capillary with homeotropic anchoring conditions for  $\mathbf{n}$  on the lateral boundary. We confirm the result found by Semenov [5] for the dependence of the quasi-static force on the separation between the defects in the case of equal elastic constants in the Oseen-Frank free-energy functional, and we extend his study to the case of unequal elastic constants. In Sec. IV, we draw the main conclusions of this work. The paper is closed by two appendices: the first concerns Ericksen's stress tensor and its expression in a reduced geometry, while the second collects for the reader's ease the essential details of the numerical method employed in Sec. III to compute the interaction force.

## II. ELASTIC FORCE

In this section we derive an explicit formula for the force exerted on a point defect by the surrounding director field. We resort to a dynamical principle, which also makes our formula valid when the director field fails to minimize the free-energy functional. The method developed here can easily be applied to disclinations with an arbitrary shape (see [6]).

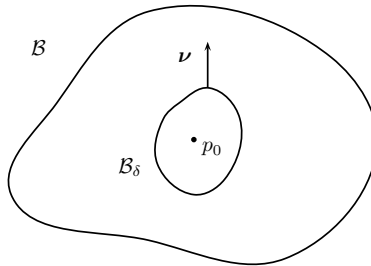


FIG. 1: Nested regions  $\mathcal{B}_\delta$  around a point defect at  $p_0$ .

### A. Force formula

Consider a director field  $\mathbf{n}$  with a point defect at  $p_0$ . We imagine to isolate  $p_0$  from the surrounding material by including it in a family of nested small regions  $\mathcal{B}_\delta$  with  $0 < \delta \leq 1$ , which shrink to  $p_0$  as  $\delta \rightarrow 0$ . For convenience, we further set  $\mathcal{B}_1 =: \mathcal{B}$  (cf. Fig. 1). The basic assumption is that the field  $\mathbf{n}$  *glides* at constant velocity  $\mathbf{v}$  in  $\mathcal{B}$ , while there is *no* mass flow, including the one that could be generated by the director reorientation (*backflow*). Formally,

$$\mathbf{n}(p, t + \varepsilon) = \mathbf{n}(p - \varepsilon \mathbf{v}, t) \quad (1)$$

for all  $p \in \mathcal{B}$  and  $\varepsilon$  sufficiently small. Likewise, since  $\mathbf{v}$  is taken to be constant,

$$\nabla \mathbf{n}(p, t + \varepsilon) = \nabla \mathbf{n}(p - \varepsilon \mathbf{v}, t). \quad (2)$$

It follows from Eqs. (1) and (2) that

$$\dot{\mathbf{n}} = -(\nabla \mathbf{n})\mathbf{v}, \quad (\nabla \mathbf{n})\dot{\phantom{a}} = -(\nabla^2 \mathbf{n})\mathbf{v}, \quad (3)$$

where the dot represents differentiation with respect to time. In the absence of mass flow, the motion in  $\mathcal{B} \setminus \mathcal{B}_\delta$ , for a given  $\delta$ , is governed by the dissipation principle that states that

$$-\mathcal{W}_\delta + \mathcal{W} = \dot{\mathcal{F}} + \mathcal{D}, \quad (4)$$

where  $\dot{\mathcal{F}}$  is the time rate of the free energy stored in  $\mathcal{B} \setminus \mathcal{B}_\delta$ ,  $\mathcal{W}_\delta$  and  $\mathcal{W}$  are the power expended by the contact torques acting on  $\mathbf{n}$  at the boundary of  $\mathcal{B}_\delta$  and  $\mathcal{B}$ , respectively, and  $\mathcal{D}$  is the energy dissipated in  $\mathcal{B} \setminus \mathcal{B}_\delta$  (see [7]).

For general liquid crystals,  $\mathcal{F}$  and  $\mathcal{W}_\delta$  are given the following expressions (see [4] and [7]):

$$\mathcal{F} = \int_{\mathcal{B} \setminus \mathcal{B}_\delta} \sigma(\mathbf{n}, \nabla \mathbf{n}) dv$$

and

$$\mathcal{W}_\delta = \int_{\partial\mathcal{B}_\delta} \mathbf{L}\boldsymbol{\nu} \cdot \mathbf{w} \, da, \quad (5)$$

where  $\boldsymbol{\nu}$  denotes the outer unit normal to  $\mathcal{B}_\delta$ ,  $\mathbf{w}$  is the local angular velocity of  $\mathbf{n}$  defined by

$$\mathbf{w} := \mathbf{n} \times \dot{\mathbf{n}}, \quad (6)$$

and

$$\mathbf{L} := \mathbf{W} \frac{\partial \sigma}{\partial \nabla \mathbf{n}} \quad (7)$$

is the couple stress tensor, with  $\mathbf{W}$  the skew symmetric tensor associated with  $\mathbf{n}$ , so that  $\mathbf{W}\mathbf{u} = \mathbf{n} \times \mathbf{u}$ , for all vectors  $\mathbf{u}$ . Moreover,

$$\mathcal{D} = \gamma_1 \int_{\mathcal{B} \setminus \mathcal{B}_\delta} \dot{\mathbf{n}}^2 \, dv,$$

where  $\gamma_1$  is the *rotational viscosity*.

By use of Eq. (3),  $\dot{\mathcal{F}}$  can be expressed as

$$\dot{\mathcal{F}} = - \int_{\mathcal{B} \setminus \mathcal{B}_\delta} \mathbf{v} \cdot \left( (\nabla \mathbf{n})^T \frac{\partial \sigma}{\partial \mathbf{n}} + \frac{\partial \sigma}{\partial \nabla \mathbf{n}} : \nabla^2 \mathbf{n} \right) \, dv = - \int_{\mathcal{B} \setminus \mathcal{B}_\delta} \mathbf{v} \cdot \nabla \sigma \, dv,$$

where in Cartesian components

$$\left( \frac{\partial \sigma}{\partial \nabla \mathbf{n}} : \nabla^2 \mathbf{n} \right)_h = \left( \frac{\partial \sigma}{\partial \nabla \mathbf{n}} \right)_{ij} n_{i,jh}.$$

Similarly, by inserting Eq. (7) into (5), since by (6)

$$\mathbf{W}^T \mathbf{w} = -\mathbf{n} \times \mathbf{w} = \dot{\mathbf{n}},$$

we arrive at

$$\mathcal{W}_\delta = - \int_{\partial\mathcal{B}_\delta} \mathbf{v} \cdot (\nabla \mathbf{n})^T \frac{\partial \sigma}{\partial \nabla \mathbf{n}} \boldsymbol{\nu} \, da.$$

On the other hand, again by Eq. (3),

$$\mathcal{D} = \gamma_1 \int_{\mathcal{B}} \mathbf{v} \cdot (\nabla \mathbf{n})^T (\nabla \mathbf{n}) \mathbf{v} \, dv.$$

Thus, Eq. (4) becomes

$$- \int_{\partial\mathcal{B}_\delta} \mathbf{v} \cdot \mathbf{T}\boldsymbol{\nu} \, da + \int_{\partial\mathcal{B}} \mathbf{v} \cdot \mathbf{T}\boldsymbol{\nu} \, da = \gamma_1 \int_{\mathcal{B} \setminus \mathcal{B}_\delta} \mathbf{v} \cdot (\nabla \mathbf{n})^T (\nabla \mathbf{n}) \mathbf{v} \, dv, \quad (8)$$

where

$$\mathbf{T} := \sigma \mathbf{I} - (\nabla \mathbf{n})^T \frac{\partial \sigma}{\partial \nabla \mathbf{n}} \quad (9)$$

is the *elastic* part of Ericksen's stress tensor for liquid crystals [8]. A uniform hydrostatic pressure could systematically be added to  $\mathbf{T}$ , as it would have no effect on either the equilibrium equations or the resultant forces computed below (cf. Appendix A).

The mechanical interpretation of Eq. (8) is rather transparent: the integrals over  $\partial\mathcal{B}_\delta$  and  $\partial\mathcal{B}$  represent the power expended by the contact forces acting on the boundary of  $\mathcal{B} \setminus \mathcal{B}_\delta$ , while a *virtual* flow conveys  $\mathbf{n}$  in a constant drift; the total power equals the total dissipation, as no internal energy is associated with a constant drift. In particular, in the limit as  $\delta \rightarrow 0$ ,

$$-\lim_{\delta \rightarrow 0} \int_{\partial\mathcal{B}_\delta} \mathbf{v} \cdot \mathbf{T}\boldsymbol{\nu} \, da$$

represents the power expended by a concentrated force  $-\mathbf{f}$  exerted on  $\mathcal{B}$  at  $p_0$ . Clearly, the force  $\mathbf{f}$  acting *on* the defect at  $p_0$  is then

$$\mathbf{f} = \lim_{\delta \rightarrow 0} \int_{\partial\mathcal{B}_\delta} \mathbf{T}\boldsymbol{\nu} \, da. \quad (10)$$

Though no mass flow is present in  $\mathcal{B} \setminus \mathcal{B}_\delta$ , which makes the contact forces expend no power in Eq. (4), the force  $\mathbf{f}$  on the defect just balances these forces. This means that in liquid crystals all forces, including those acting on defects, are represented by Ericksen's stress tensor  $\mathbf{T}$ , and so no need arises of defining any analogue of Eshelby's tensor for configurational forces [9, 10].

The formula for the force acting on a point defect is the same also if  $\mathbf{v}$  is not constant. In this case, Eq. (3)<sub>2</sub> would be replaced by

$$(\nabla \mathbf{n}) \dot{\phantom{\mathbf{n}}} = -(\nabla^2 \mathbf{n})\mathbf{v} - (\nabla \mathbf{n})(\nabla \mathbf{v}),$$

and as a result, the integral

$$\int_{\mathcal{B} \setminus \mathcal{B}_\delta} \mathbf{T} \cdot \nabla \mathbf{v} \, dv \quad (11)$$

should be added on the right-hand side of Eq. (8). Interpreting Eq. (11) as the power expended by the internal forces in the virtual flow  $\mathbf{v}$ , we arrive at the same expression for  $\mathbf{f}$  as in Eq. (10).

Equation (10) is essentially the same as the one derived by Eshelby in [10] for the quasi-static force on a nematic disclination—see Appendix A for a generalized derivation of Eshelby's formula. We learn here that in the absence of backflow the elastic force on a defect is delivered by the same expression in both dynamics and quasi-statics: the outcomes can, however, be quite different in the two cases, as the stress tensors need not coincide.

Finally, let  $\delta$  be given. Were  $\mathcal{B}_\delta$  a solid particle immersed in the liquid crystal with strong anchoring of the director  $\mathbf{n}$  on  $\partial\mathcal{B}_\delta$ , the total elastic force exerted on  $\mathcal{B}_\delta$  would be expressed as

$$\int_{\partial\mathcal{B}_\delta} \mathbf{T}\boldsymbol{\nu} \, da.$$

In this case, however, the *real* flow connected with the motion of  $\mathcal{B}_\delta$  could not be neglected. We note that by Eq. (10) the force on the solid particle above can be viewed as an approximation to the force on the defect,  $\mathbf{f}$ .

### B. Axisymmetric director fields

Formula (10) for the force on a defect can be given a simpler form when the director field  $\mathbf{n}$  is symmetric about an axis, with the defect lying on it. In this case it is convenient to employ cylindrical co-ordinates  $(r, \vartheta, z)$ , with  $z$  along the symmetry axis. We further restrict  $\mathbf{n}$  to be represented as

$$\mathbf{n} = \cos \psi \mathbf{e}_r + \sin \psi \mathbf{e}_z, \quad (12)$$

where  $\psi$  is a function of  $r$  and  $z$ . The free-energy density  $\sigma$  can then be expressed as a function of  $\psi$  and its gradient  $\nabla\psi = \psi_{,r}\mathbf{e}_r + \psi_{,z}\mathbf{e}_z$ ; moreover (see Appendix A),

$$\mathbf{T} = \sigma\mathbf{I} - \nabla\psi \otimes \frac{\partial\sigma}{\partial\nabla\psi}. \quad (13)$$

By symmetry,  $\mathbf{f} = f_z\mathbf{e}_z$ . Taking for  $\mathcal{B}_\delta$  a ball with radius  $\delta$  centered in the defect, we can write

$$f_z = \lim_{\delta \rightarrow 0} f_z(\delta), \quad (14)$$

where

$$f_z(\delta) := 2\pi \int_{\mathcal{C}_\delta} \mathbf{e}_z \cdot \mathbf{T}\boldsymbol{\nu} r \, ds, \quad (15)$$

with  $\mathcal{C}_\delta$  the semi-circular arc of radius  $\delta$  around the defect in an  $(r, z)$ -plane cross-section of the region occupied by the liquid crystal. Setting  $\boldsymbol{\nu} = \nu_r\mathbf{e}_r + \nu_z\mathbf{e}_z$ , since

$$\frac{\partial\sigma}{\partial\nabla\psi} = \frac{\partial\sigma}{\partial\psi_{,r}}\mathbf{e}_r + \frac{\partial\sigma}{\partial\psi_{,z}}\mathbf{e}_z,$$

by Eq. (13) we arrive at

$$\mathbf{e}_z \cdot \mathbf{T}\boldsymbol{\nu} = -\left(\frac{\partial\sigma}{\partial\psi_{,r}}\psi_{,z}\right)\nu_r + \left(\sigma - \frac{\partial\sigma}{\partial\psi_{,z}}\psi_{,z}\right)\nu_z, \quad (16)$$

which is to be used in Eq. (15).

### III. DEFECT INTERACTION IN A CAPILLARY

The quasi-static force acting on a defect can be computed at least in two ways: by minimizing the total free energy  $\mathcal{F}$  with the defect held fixed and then differentiating  $-\mathcal{F}$  with respect to the position of the defect, or by evaluating formula (10) on a sequence of regions  $\mathcal{B}_\delta$  shrinking to the defect. It is shown in Appendix A that these two ways are indeed equivalent—in the quasi-static setting. More specifically, since the divergence of Ericksen’s stress tensor vanishes on all configurations that minimize  $\mathcal{F}$ , including those with constrained defects, the limit in Eq. (10) need not be computed, as the integral in Eq. (10) does not depend on the specific region  $\mathcal{B}_\delta$  in the shrinking family. In a dynamic setting, however, this limit must be computed, because Ericksen’s tensor fails in general to be divergence-free. We elaborated a method to compute the limit of Ericksen’s traction, and here we apply it to quasi-static forces that have already been computed independently. Comparing our outcomes with existing results will make us confident in the validity of our method, which is to prove especially useful in dynamics.

Below we study the problem of the interaction of a pair of point defects of opposite topological charge in a capillary. Thus we consider a  $+1$  defect (hedgehog) and a  $-1$  defect (anti-hedgehog) separated some finite distance along the axis of an infinite cylindrical capillary with homeotropic anchoring. We employ Oseen-Frank’s general formula for the free-energy density:

$$\sigma = k_1(\operatorname{div} \mathbf{n})^2 + k_2(\mathbf{n} \cdot \operatorname{curl} \mathbf{n})^2 + k_3|\mathbf{n} \times \operatorname{curl} \mathbf{n}|^2 + k_{24}\sigma_{24}, \quad (17)$$

where

$$\sigma_{24} := \operatorname{tr}(\nabla \mathbf{n})^2 - (\operatorname{div} \mathbf{n})^2 = \operatorname{div}((\nabla \mathbf{n})\mathbf{n} - (\operatorname{div} \mathbf{n})\mathbf{n})$$

is a null Lagrangian, as for smooth director fields the integral of  $\sigma_{24}$  over the whole region occupied by the material depends only on the boundary data for  $\mathbf{n}$  (see, e.g., Sec. 3.8 of [11]), and so it contributes a given constant to the free-energy functional whenever this is subject only to Dirichlet boundary conditions. Also in the presence of point defects, the integral of  $\sigma_{24}$  contributes the same constant, as long as  $|\nabla \mathbf{n}|$  diverges at most like  $1/\rho$  at the distance  $\rho$  from the defect. Thus, for the problem we study,  $k_{24}$  can freely be chosen in Eq. (17) without affecting either the minimizer or the quasi-static force on the defects (see also Appendix A). Here we set  $k_{24} = k_1$ , so that  $\sigma = k|\nabla \mathbf{n}|^2$  when  $k = k_1 = k_2 = k_3$  (the

one-constant approximation). When  $\mathbf{n}$  is as in Eq. (12), there is no contribution to  $\sigma$  from the twist constant  $k_2$ , and  $\sigma$  reads as

$$\sigma = k_1(\sin \psi \psi_{,r} - \cos \psi \psi_{,z})^2 + k_3(\cos \psi \psi_{,r} + \sin \psi \psi_{,z})^2 + k_1 \frac{\cos^2 \psi}{r^2}.$$

The interaction in a capillary between two defects with opposite charge has been studied by several authors, including [5, 12]. More specifically, in [5] the one-constant approximation to the Oseen-Frank energy was used in a study that combined approximate analysis and numerical computation. A prediction was made that the force of attraction between two such defects should remain finite as the separation between them shrinks to zero; while this force decays exponentially to zero as the separation grows large.

We have several objectives in mind. First, we compare the general method in the previous section with alternate methods restricted to equilibrium settings, in particular with the approach of differentiating the (quasi-static) values of the free energy with respect to the separation between the defects, as is done in [5]. Next, we wish to explore the practical limitations of our approach. The numerical evaluation of Eq. (15) requires integration on very small surfaces enclosing singularities in the director field. It is a difficult computation, and it is of interest to know the accuracy to which these values can be obtained. Finally, we are interested in extending the analysis of [5] to the case of unequal elastic constants in order to see what new effects are obtained.

In brief, we find the following. The forces we calculate using Eqs. (14)–(16) agree with those of [5] to the degree that can be determined from the graphical data reported in that paper.

Our numerical approach delivers approximately four significant digits when the separation between the defects is moderate (0.5 to 1.5 times the radius of the cylindrical capillary) and the elastic constants are not too different. The accuracy deteriorates as the separation becomes smaller or larger, or as the ratio  $k_3/k_1$  becomes too small or too large. Below a separation of about .05 radii, it is not possible to obtain meaningful results (with our current numerical approach); while beyond a separation of about two radii, the force is essentially negligible. The forces on the different defects remain equal and opposite in sign (to the noise level of the computations) when the elastic constants are different, as should be the case in quasi-statics. As  $k_3$  increases relative to  $k_1$ , the attractive force (in units of  $k_1$ ) increases for small separations but decreases for moderate to large separations.



### A. Numerical modelling

For each fixed value of the separation between the defects, we must determine the equilibrium director field of a discretized model for our problem, evaluate the approximate forces using Eq. (15) for a sequence of decreasing  $\delta$ 's, and extract the limiting force by extrapolation to  $\delta = 0$ . Using axial symmetry and cylindrical coordinates (as in Sec. IIB), we reduce our computational problem to a finite two-dimensional region in the  $(r, z)$ -plane with far-field “escape” boundary conditions on the truncated cylinder end caps. While the singularities at the defect points are integrable (of finite energy), they are indeed singularities of the vector field, and the director and associated orientation angle  $\psi$  are not defined at these points. To accommodate this and to facilitate the evaluation of the force integrals that we require, we have adopted an approach of solving sequences of regular problems on reduced regions with small semi-circular neighborhoods of the defect points cut out of the domain. As these cut-out neighborhoods shrink to the defect points, the director fields and force integrals should converge to the proper values for the full region and true problem.

The computational domain, then, is a subset of the rectangle  $0 < r < R$ ,  $-L < z < d+L$ , where  $R$  is the radius of the capillary,  $d$  is the separation between the defect points on the axis, and  $L$  is “sufficiently large” for our far-field boundary conditions. The *defects* are located at  $(r, z) = (0, 0)$  (+1, hedgehog) and  $(0, d)$  (−1, anti-hedgehog) and are surrounded by the semi-circular excluded cutouts. The computational domain,  $\Omega$ , is depicted in Fig. 2.

A piecewise-linear triangular finite-element method is used to solve a weak formulation of the equilibrium problem for  $\psi$ . This allows for the use of graded meshes (which are needed here) and better adaptation to the curved parts of the boundary. Dirichlet boundary conditions are imposed on  $r = 0$  where  $\psi = \pm\pi/2$ ,  $r = R$  where  $\psi = 0$ , and the end caps  $z = -L$ ,  $d + L$  where  $\psi$  is the appropriate “escape” solution of Cladis and Kléman [13]. The angle  $\psi$  is free on the boundaries of the small cutouts, this resulting in the appropriate natural boundary condition. Thus we seek a function  $\psi(r, z)$  that conforms to the Dirichlet boundary conditions and satisfies

$$\iint_{\Omega} \left\{ \frac{\partial \sigma}{\partial \nabla \psi}(\psi, \nabla \psi) \cdot \nabla \varphi + \frac{\partial \sigma}{\partial \psi}(\psi, \nabla \psi) \varphi \right\} r \, dr \, dz = 0$$

for all test functions  $\varphi$  that vanish on the Dirichlet boundaries.

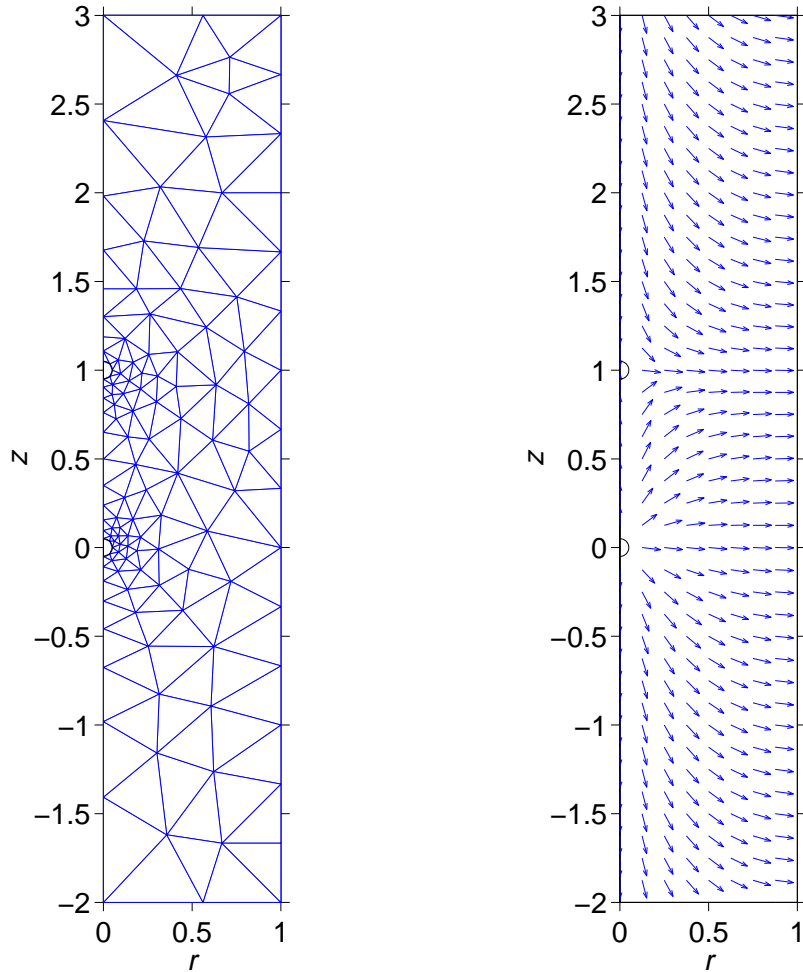


FIG. 2: Initial, coarse mesh (left); calculated director field on refined mesh (right). Geometric parameters:  $R = d = 1$ ,  $L = 2$ ,  $\delta = .05$ . Coarse mesh parameters: 207 triangles, 131 vertices.

We have utilized the finite element package PLTMG [14]. It allows for circular arcs as “triangle” edges and properly handles such elements with its quadratures. It also allows for the evaluation of auxiliary functionals, which may contain boundary line integrals. It approximates such integrals using a quadrature rule, with values for  $\psi$ ,  $\psi_r$ , and  $\psi_z$  interpolated from the adjacent triangle. We employ this to evaluate our force integrals.

We use a sequence of graded meshes each of which puts twice as many triangle edges around each of the semi-circular cutouts  $\mathcal{C}_\delta$  (where the director turns by  $\pi$ ) as along each of the end caps (where the director rotates half as much). The initial finite-element triangulation is automatically generated by the package from primitive geometric input from the user. It can be controlled to some extent via user-defined parameters. We refine the

finite element meshes by uniform quadrisection. The finest meshes typically contain on the order of 160,000 triangles and 80,000 vertices. Data are collected for all refinement levels and extrapolated to zero mesh width (for each fixed  $\delta$ ). These mesh-extrapolated values are subsequently extrapolated to  $\delta \rightarrow 0$ . An initial coarse mesh and a computed solution (on a finer mesh) are depicted in Fig. 2.

The solver in the package uses a very efficient algorithm of multigrid type; with the good initial guesses provided by the sequence of refinements and solves, it takes only a minute or so on a modern PC to solve the nonlinear system of equations on the finest mesh. This is very helpful since the order of convergence of the quadrature approximation to the force integrals proves to be only  $O(h)$  (because of the singularities), and so these very refined meshes (and very large systems of equations to solve) are truly necessary in order to obtain acceptable accuracy. Additional details concerning benchmarking of the code can be found in Appendix B.

## B. Interaction force

We have used the numerical approach described above to study the force of attraction between the two defects as a function of the distance between them. Our non-dimensionalization expresses the forces in units of  $k_1$ , lengths in units of  $R$ , and leaves as the only relevant dimensionless parameter the elastic-constant ratio  $k_3/k_1$ . Our main point of comparison is with the numerical results reported in [5] for the equal-elastic-constant case, in particular with Fig. 2 of that paper. Our numerical results for this case are plotted as the solid line in Fig. 3 and agree to the level of discernment with those in [5]—note that the units differ between the two papers ( $K = 2k_1$  and  $D = 2R$ ). We also find a good agreement for the limit of the force as  $d \rightarrow 0$ :  $8\pi \doteq 25.1327$  versus our numerically obtained value of 25.16.

We have extended the analysis of this problem in both the numerical and analytical aspects to the case of unequal elastic constants. In Fig. 3, we plot the force curves for the values  $k_3/k_1 = 0.5$  and  $2.0$  (in addition to  $k_3/k_1 = 1.0$ ). We find that as the ratio  $k_3/k_1$  is increased, the attractive force (in units of  $k_1$ ) increases near annihilation but decreases for moderate to large separations; this latter aspect is somewhat non-intuitive and is discussed below.

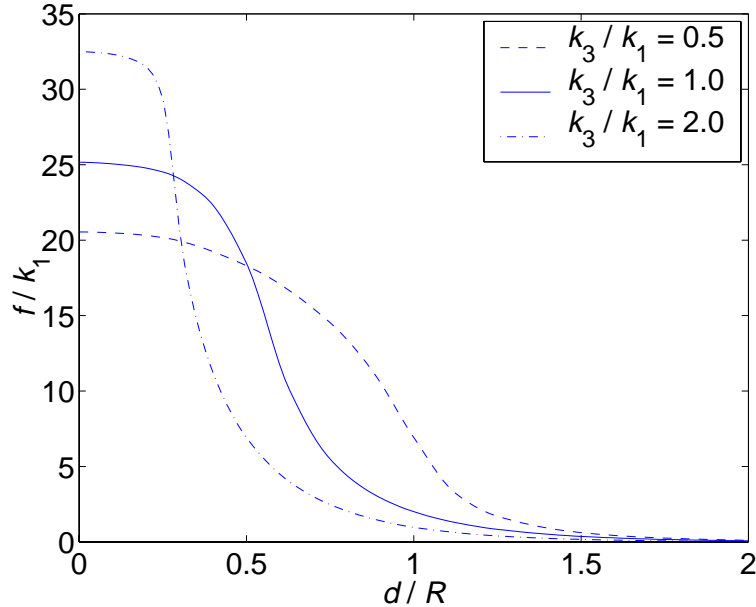


FIG. 3: Numerically calculated forces of attraction between a hedgehog and an anti-hedgehog in a capillary.  $f$  denotes the force;  $k_1$  and  $k_3$  are the splay and bend elastic constants;  $d$  is the separation between the defects; and  $R$  is the radius of the capillary.

$k_3/k_1$	formula (18)	numerical
0.5	20.3980	20.54
1.0	25.1327	25.16
2.0	32.3056	32.49

TABLE I: Comparison of limiting forces (as separation  $d \rightarrow 0$ ) predicted by Eq. (18) with numerically computed values. The forces are in units of  $k_1$ .

We can understand several features of Fig. 3. At short separations, the greater forces observed for larger values of  $k_3/k_1$  are to be expected, simply on the grounds of stronger elasticity. One also observes that the three force curves tend to become flat (each forming a plateau) as  $d \rightarrow 0$ . This indicates that when the separation between the defects is sufficiently small compared to  $R$ , they behave as if they were in free space, with no boundary condition imposed on the director field. In free space, the interaction energy is directly proportional to the distance between the defects, and so the force is in fact constant (as first indicated in [15] and [16]). This conclusion is rigorously reached by computing the *infimum* of the free

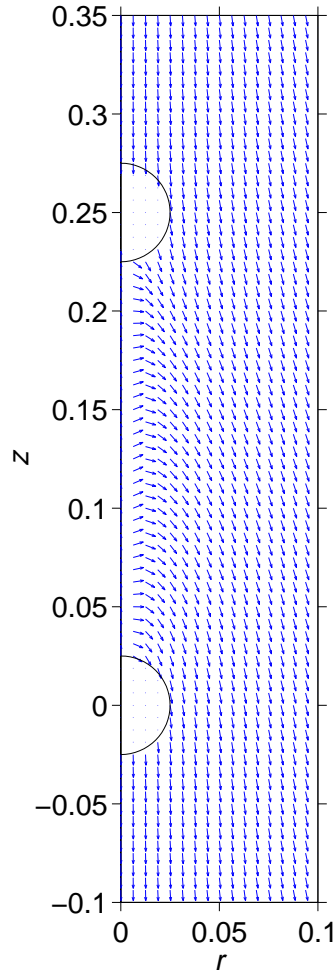


FIG. 4: Magnified view of the equilibrium director field at a short separation between the defects. Parameters:  $k_3 = k_1$ ,  $d = .25R$ . There is a clear indication of the onset of the scaling regime.

energy with fixed point defects, which actually fails to be attained (as proved in [17, 18] for the one-constant approximation). Qualitatively, the interaction energy between two defects results from a huge concentration of elastic distortion in a narrow strip joining the defects, where  $\mathbf{n}$  turns by  $\pi$ ; this strip eventually shrinks to a string in the limit where the infimum of the energy is approached. There is indeed a great deal of distortion of the director field for our problem at very narrow separations, as is illustrated in Fig. 4, where  $\mathbf{n}$  turns almost by  $\pi$  in a narrow region between the defects, and this makes the numerical code become quite strained.

The existence of this “scaling regime” has led us to derive a formula for the limiting value of the force (as the separation goes to zero) that is valid for elastic constants that are not

necessarily equal:

$$f(0+) = 4\pi k_1 \begin{cases} 1 + \frac{k}{\sqrt{1-k}} \ln \frac{\sqrt{1-k} + 1}{\sqrt{k}}, & k_3 < k_1 \\ 2, & k_3 = k_1 \\ 1 + \frac{k}{\sqrt{k-1}} \arcsin \sqrt{\frac{k-1}{k}}, & k_3 > k_1 \end{cases}, \quad k := \frac{k_3}{k_1}. \quad (18)$$

The derivation and consideration of this formula will be presented elsewhere. In Table I we indicate that the limiting values we compute with our code agree to the noise level with those predicted by this formula.

The inverted behavior of the three curves for  $d > .5R$  is surprising at first encounter. We attribute the stronger attractive force associated with smaller values of  $k_3/k_1$  to the fact that decreasing  $k_3$  relative to  $k_1$  tends to localize more the distortion near the cylinder axis. The onset of the scaling regime depends on the elastic constants: it takes place at larger values of  $d$  when  $k_3/k_1$  is smaller. This is a sign that for smaller values of  $k_3/k_1$  the boundary conditions are less effective in preventing the elastic distortion of the director to be concentrated in the region of the axis between the defects, where the bend contribution is large. As the scaling regime prevails, the strength of the interaction increases because the director configuration becomes closer to the string concentration to which the highest force pertains. This is illustrated in Fig. 5. This same argument also illuminates the different ordering of the forces for a small separation between the defects. While the director arrangement would essentially be the same  $\pi$  turn in all cases, the energy, and so the force, increases with  $k_3$  because of the increased cost of the bend, as implied by being  $f(0+)$  in Eq. (18) monotonic in  $k$ .

All three force curves exhibit well-defined exponential decays, with asymptotic decay rates of 3.2, 3.14, and 3.5 (for  $k_3/k_1 = 0.5, 1.0,$  and  $2.0$ ) versus  $d/R$ . We conjecture that the actual decay rate for the equal-elastic-constants case is  $\pi$ . For all three forces, the values at  $d = 2R$  are less than roughly .5% of their maximum values (obtained in the limit  $d \rightarrow 0$ ). The ‘‘cutoff point’’ (the point beyond which the interaction force is effectively zero) found and utilized in [12] was  $d = 2.2R$ , which for our three numerically generated force laws corresponds to values no greater than .3% of their maximums.

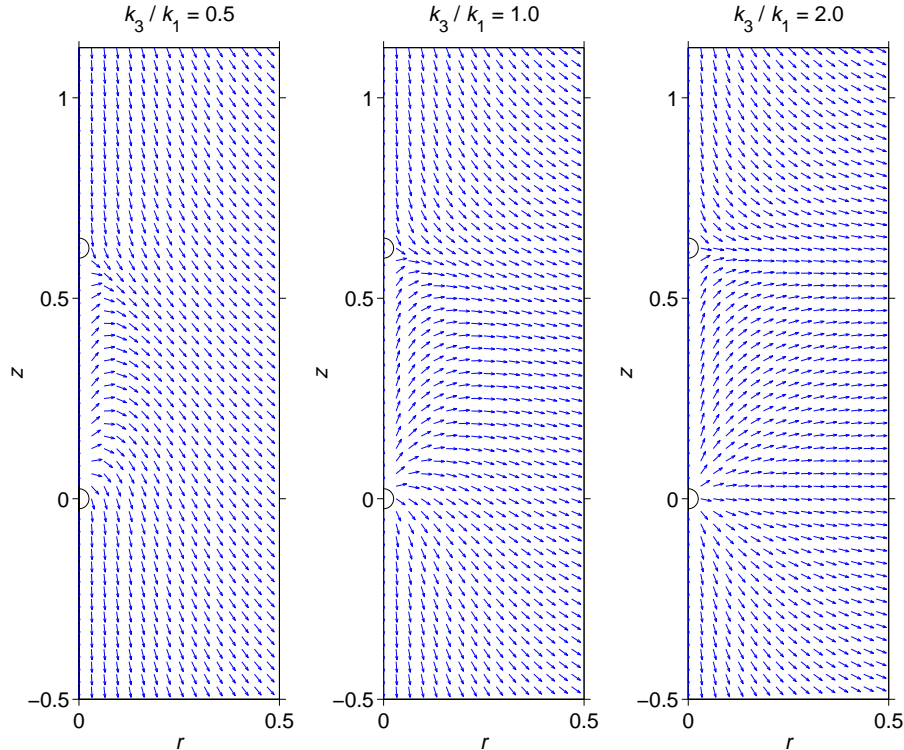


FIG. 5: Equilibrium director fields (on a sub-region) at a separation of  $d = .625R$  for three different elastic-constant ratios:  $k_3/k_1 = 0.5$  (left),  $1.0$  (center), and  $2.0$  (right). At this separation, the three associated forces differ significantly.

#### IV. DISCUSSION

We derived an expression that allows one to compute the elastic force on a nematic defect directly from the director field close to the defect: it is obtained by integrating the traction of Ericksen's stress tensor over the surface of neighborhoods shrinking to the defect. Though here material flow has been neglected, this force is the same as the purely elastic force felt by a small particle subject to flow with fixed director on its boundary.

The force found is essentially the same derived by Eshelby using a quasi-static approach. However, there are serious restrictions to quasi-statics. For example, in a geometry with translational symmetry, the equilibrium free energy of two point defects can depend only on the distance between them. Hence the forces on the defects obtained by differentiating the free energy with respect to the defect positions are necessarily equal and opposite. Moreover, the divergence of Ericksen's stress  $\mathbf{T}$  vanishes in quasi-statics, and so the force on a defect

is delivered by computing the integral of the traction  $\mathbf{T}\boldsymbol{\nu}$  on any region  $\mathcal{B}_\delta$  that encloses only that defect. In contrast, the method presented here is not restricted to equilibrium director fields; it could deliver forces that in the dynamic annihilation of a defect pair might fail to sum to zero. Even with equal and opposite forces, still dissipation or backflow might account for the asymmetries observed by Cladis and Brand [2].

This achievement is a major step towards the understanding of defect dynamics. There are, however, some issues that still need to be addressed to obtain a complete picture. Apart from the flow effects, it would be necessary to include the dissipation connected with the defect motion. If it were possible to determine the dissipation merely from the behavior of the director field close to the defect, as is the case for the elastic force, the dissipation would result in an effective mass. It appears, however, that this is not feasible, due to the non-local nature of the dissipation.

To show the validity of our method, we have applied it to a standard problem: computing the quasi-static forces felt by two point defects in a capillary with homeotropic anchoring. For equal splay and bend elastic constants, we found essentially the same results reported in [5]. The distance dependence of the force changed with the ratio  $k_3/k_1$ , while, as expected, forces remained always equal and opposite. With decreasing  $k_3$ , the director distortion becomes more concentrated in the region of the axis between the two defects, which results in a stronger binding of the defects at moderate to large distances. The integral of the force curve represents the total work done in the annihilation process and is less sensitive to the ratio of the elastic constants. In fact, it represents the energy barrier to be overcome in transforming one escaped state into the opposite one by nucleating and expelling a pair of defects. We also found that when the defect separation is small enough, the force approaches the value pertaining to the interaction in free space: the existence of such a “scaling regime” has here been established also in the case of unequal elastic constants.

While the method presented here achieves a satisfactory accuracy, it is somewhat difficult to implement and the evaluation of the force integrals requires some special attention. Though, as we have shown, this method can be applied to the computation of quasi-static forces, the classical method relying on differentiation of the free energy could in some cases be more effective. The strengths of our approach lie in its applicability to dynamic problems and in the fact that one can arrive directly at the force without performing the integration necessary to compute the total free energy. This can be particularly important for



computations where the director field is known, but the integration cannot be carried out.

### Acknowledgments

The first author gratefully acknowledges the support of the National Science Foundation grants DMR 89-20147 and DMS-0107761.

### APPENDIX A: ERICKSEN'S STRESS TENSOR

In this Appendix we derive the general expression of Ericksen's stress tensor for liquid crystals by performing a *domain* variation of the free-energy functional. This proves useful in extending to point defects the original derivation of Eshelby [10] for the quasi-static force on a disclination.

Consider the same family of nested regions  $\mathcal{B}_\delta$  in Fig. 1. Let  $\mathbf{n}$  be a director field with a point defect at  $p_0$  that minimizes the free-energy functional  $\mathcal{F}$  subject to strong anchoring conditions on  $\partial\mathcal{B}$ .  $\mathcal{F}$  must be stationary at  $\mathbf{n}$  also relative to domain variations (cf. Sec. 5.2 of [11]). One such variation is obtained as follows. For a given positive  $\varepsilon$ , let  $\mathcal{B}$  be mapped into itself by the deformation defined by  $\mathcal{B} \ni p \mapsto p_\varepsilon = p + \varepsilon\mathbf{u}$ , where  $\mathbf{u}$  vanishes on  $\partial\mathcal{B}$ . A domain variation of  $\mathbf{n}$  is the field  $\mathbf{n}_\varepsilon$  that satisfies the equation

$$\mathbf{n}_\varepsilon(p_\varepsilon) = \mathbf{n}(p) \quad \text{for all } p \in \mathcal{B}; \quad (\text{A1})$$

accordingly,

$$\nabla\mathbf{n}_\varepsilon = \nabla\mathbf{n}(\mathbf{I} - \varepsilon\nabla\mathbf{u}) + o(\varepsilon). \quad (\text{A2})$$

By use of these equations, we easily arrive at the corresponding domain variation of  $\mathcal{F}$ :

$$\begin{aligned} \frac{d}{d\varepsilon} \left( \mathcal{F}[\mathbf{n}_\varepsilon] \right)_{\varepsilon=0} &= \frac{d}{d\varepsilon} \left( \int_{\mathcal{B} \setminus \mathcal{B}_\delta} \sigma(\mathbf{n}, \nabla\mathbf{n} - \varepsilon\nabla\mathbf{n}\nabla\mathbf{u})(1 + \varepsilon \operatorname{div} \mathbf{u}) \, dv \right)_{\varepsilon=0} \\ &= - \int_{\partial\mathcal{B}_\delta} \mathbf{T}\boldsymbol{\nu} \cdot \mathbf{u} \, da - \int_{\mathcal{B} \setminus \mathcal{B}_\delta} \operatorname{div} \mathbf{T} \cdot \mathbf{u} \, dv, \end{aligned} \quad (\text{A3})$$

where  $\mathbf{T}$  is as in Eq. (9) and both integrations by parts and the divergence theorem have been employed. Taking the limit as  $\delta \rightarrow 0$  in Eq. (A3), while the defect is being held fixed ( $\mathbf{u}(p_0) = \mathbf{0}$ ), one concludes by the arbitrariness of  $\mathbf{u}$  that the equilibrium equation for  $\mathbf{n}$  is (see also [8])

$$\operatorname{div} \mathbf{T} = \mathbf{0} \quad \text{in } \mathcal{B} \setminus p_0. \quad (\text{A4})$$

When the same limit is taken on a director field satisfying Eq. (A4), but with  $\mathbf{u}(p_0)$  arbitrary, we obtain from Eq. (A3) the same expression as in (10) for what is now to be interpreted as the *quasi-static* force on the defect. This is the essence of Eshelby’s reasoning in [10]. Our paper, building upon a dynamical principle, shows that Eq. (10) also applies to the dynamic elastic force on a point defect.

Another consequence of Eq. (A3) is that null Lagrangians do not affect the quasi-static force on a point defect, as long as they contribute a constant to the total elastic free energy. This, however, is a property inherited from the equilibrium configurations, which need not apply to the dynamic elastic force.

Whenever the director field  $\mathbf{n}$  can be described in terms of a single scalar function  $\psi$  [as, for example, in Eq. (12)], instead of computing  $\mathbf{T}$  directly through Eq. (9), it is easier to arrive at an alternative expression for it by performing a domain variation of  $\psi$ . Equations (A1) and (A2) are thus replaced by

$$\psi_\varepsilon(p_\varepsilon) = \psi(p)$$

and

$$\nabla\psi_\varepsilon = (\mathbf{I} - \varepsilon\nabla\mathbf{u})^T\nabla\psi + o(\varepsilon),$$

respectively. It is then easy to show that Eq. (A3) is still formally valid, but with  $\mathbf{T}$  as in Eq. (13).

## APPENDIX B: NUMERICAL DETAILS

Some numerical tests were conducted in order to ascertain the accuracy that can be achieved in calculating the forces  $f_z^\pm$  in this way. The indications are that roughly four significant digits are computed in the “well behaved” regions of the parameter space. Most of the calculations are done with  $R = k_1 = 1$ , which is equivalent to expressing lengths in units of  $R$ , forces in units of  $k_1$ , with  $k_3 \mapsto k_3/k_1$ .

### *Convergence of the force integrals*

We parameterize the meshes in a given sequence of mesh refinements (for a fixed  $\delta$ ) by the maximum triangle diameter  $h$  and denote by  $f_z^h(\delta)$  the calculated quadrature rule

approximation to  $f_z(\delta)$ , defined in Eq. (15)—here we can be referring to either defect. By examining extrapolation tables (and estimated errors and their ratios), we observe clear indications of an asymptotic error expansion of the form

$$f_z^h(\delta) = f_z(\delta) + c_1 h + c_2 h^2 + \dots ,$$

where the constants  $c_1, c_2, \dots$  do not depend on  $h$ . While it is not possible to collect enough data to validate the higher-order terms, the first two terms ( $O(h)$  and  $O(h^2)$ ) are clearly supported by the numerical evidence, in the well-behaved cases.

#### *Dependence on the mesh*

We examined the degree to which these calculations depend upon the initial mesh. Refinements and extrapolations were performed for the same set of parameters, but with different initial meshes with different mesh-grading parameters, one with 171 triangles, the other with 139. The results are displayed in Fig. 6. While the calculated values for each mesh refinement differ noticeably between the two cases, the extrapolated values are very steady, differing by two parts in the 4th decimal (suggesting that this is the noise level).

#### *Dependence on $L$*

Calculations were performed with several different values of  $L$  in order to determine an adequate size to match the intrinsic error in our discretization and extrapolation processes. On the basis of the data in Table II, it was decided to use  $L = 2.0$  for data collection.

#### *Dependence on $\delta$*

The dependence of the calculated force values on  $\delta$  is influenced by several factors, including the separation between the defects, the elastic-constant ratio, and the quality of the mesh extrapolation. The data behave regularly down to a certain point (the noise level), which may be different in different cases; after that they oscillate around some average value in a benign way. This is illustrated in Table III in a specific instance. In collecting data, we typically calculate the forces for at least three different values of  $\delta$  (e.g., .06, .03, and .015

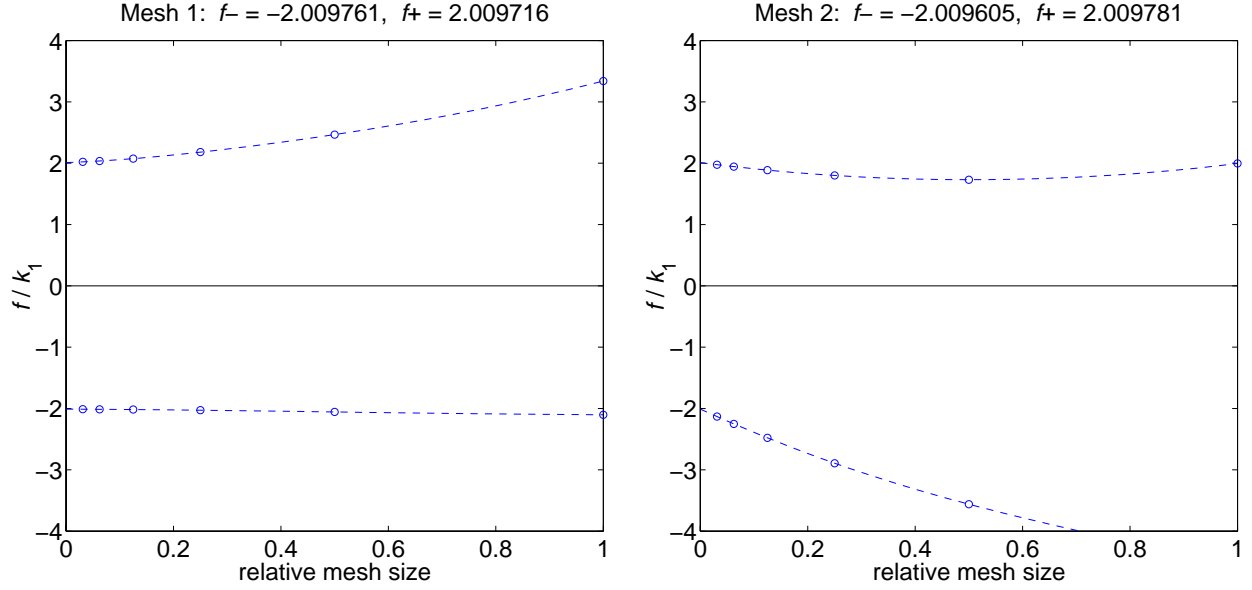


FIG. 6: Calculated forces on defects for two different initial meshes: 171 triangles (left), 139 triangles (right). Parameters:  $R = d = 1$ ,  $L = 1.5$ ,  $k_1 = k_3 = 1$ ,  $\delta = .1$ . Extrapolated values are in the titles.

$L$	$f_z^-$	$f_z^+$
1.00	-2.0748	2.0746
1.25	-2.0187	2.0176
1.50	-2.0070	2.0069
1.75	-2.0044	2.0045
2.00	-2.0040	2.0039
2.25	-2.0038	2.0038
2.50	-2.0038	2.0037

TABLE II: Dependence of calculated force values on cylinder-height parameter  $L$ . Fully mesh-extrapolated values. Parameters:  $R = d = 1$ ,  $k_1 = k_3 = 1$ ,  $\delta = .05$ .

times  $R$ ) and extrapolate if an appropriate trend behavior is exhibited or estimate the value

$\delta$	$f_z^-$	$f_z^+$
.10	-2.0069	2.0066
.09	-2.0057	2.0057
.08	-2.0042	2.0049
.07	-2.0045	2.0044
.06	-2.0041	2.0043
.05	-2.0040	2.0039
.04	-2.0039	2.0038
.03	-2.0037	2.0035
.02	-2.0039	2.0037
.01	-2.0038	2.0043

TABLE III: Dependence of calculated force values on cutout-radius parameter  $\delta$ . Fully mesh-extrapolated values. Parameters:  $R = d = 1$ ,  $L = 2$ ,  $k_1 = k_3 = 1$ .

if the indications are that the noise level has been reached.

- 
- [1] A. Pargellis, N. Turok, and B. Yurke, Phys. Rev. Lett. **67**, 1570 (1991).
- [2] P. E. Cladis and H. R. Brand, Private Communication, 2000.
- [3] J. L. Ericksen, Trans. Soc. Rheol. **5**, 23 (1961).
- [4] F. M. Leslie, Arch. Rational Mech. Anal. **28**, 265 (1968).
- [5] A. N. Semenov, Europhys. Lett. **46**, 631 (1999).
- [6] R. Rosso and E. G. Virga, in *Defects in Liquid Crystals: Computer Simulations, Theory and Experiments*, edited by O. D. Lavrentovich, P. Pasini, C. Zannoni, and S. Zumer (Kluwer, Dordrecht, 2001).
- [7] F. M. Leslie, Continuum Mech. Thermodyn. **4**, 167 (1992).
- [8] J. L. Ericksen, Arch. Rat. Mech. Anal. **9**, 371 (1962).
- [9] J. L. Ericksen, ZAMM **46**, S247 (1995).
- [10] J. D. Eshelby, Phil. Mag. A **42**, 359 (1980).
- [11] E. G. Virga, *Variational theories for liquid crystals*. (Chapman & Hall, London, 1994).

- [12] G. Guidone Peroli and E. G. Virga, *Phys. Rev. E* **54**, 5235 (1996).
- [13] P. E. Cladis and M. Kléman, *J. Phys. (Paris)* **33**, 591 (1972).
- [14] R. E. Bank, *PLTMG: A Software Package for Solving Elliptic Partial Differential Equations: User's Guide 8.0.* (SIAM, Philadelphia, 1998).
- [15] S. Ostlund, *Phys. Rev. B* **24**, 485 (1981).
- [16] W. F. Brinkman and P. E. Cladis, *Physics Today* **35**, 48 (1982).
- [17] H. Brezis, J. M. Coron, and E. Lieb, *CRAS Paris* **303**, 207 (1986).
- [18] H. Brezis, J. M. Coron, and E. Lieb, *Comm. Math. Phys.* **107**, 647 (1986).